Indocyanine Green-Loaded Photoacoustic Nanodroplets: Dual Contrast Nanoconstructs for Enhanced Photoacoustic and Ultrasound Imaging

Alexander Hannah, Geoffrey Luke, Katheryne Wilson,† Kimberly Homan, and Stanislav Emelianov*

Department of Biomedical Engineering, University of Texas at Austin, Austin, Texas 78712, United States. †Present address: Katheryne Wilson, Molecular Imaging Program and Department of Radiology, Stanford University School of Medicine, 1201 Welch, Lucas Expansion Building, Stanford, CA 94305.

ABSTRACT Recently, perfluorocarbon (PFC) nanodroplets were introduced as contrast agents for imaging and image-guided therapy. For example, in sonography, high-intensity ultrasound pulses were used to phase-transition liquid perfluorocarbon to produce gas microbubbles. More recently, perfluorocarbon nanodroplets with encapsulated gold nanorods were used as dual ultrasound/photoacoustic contrast agents. To expedite clinical translation, we synthesized and characterized ICG-loaded perfluorocarbon nanodroplets, *i.e.*, constructs comprising biocompatible, nontoxic and biologically safe materials. We then demonstrated enhanced photoacoustic contrast through optically triggered phase transition of PFC nanodroplets and ultrasound contrast from the resulting PFC bubbles. We assessed the quality enhancement of photoacoustic and ultrasound images through analysis of contrast and contrast-to-noise ratio. We further investigated the changes in image contrast due to increased ambient temperature. Our studies suggest that ICG-loaded perfluorocarbon nanodroplets may become a valuable tool for various imaging modalities, and have promising therapeutic applications.

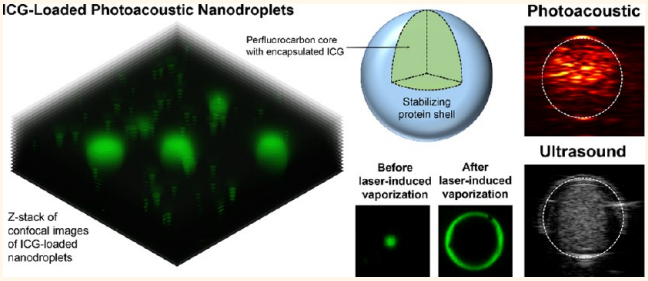

KEYWORDS: nanodroplets · perfluorocarbon · indocyanine green · imaging · vaporization · photoacoustics · ultrasound

Novel materials and constructs for imaging contrast agents are heavily researched and highly valuable to the field of medical diagnostics and image-guided therapy. Ultrasound (US) imaging is widely used clinically due to its high resolution, tissue penetration, and ability to discern soft tissues; it is portable, cost-effective, and safe for repeated use. Recently, photoacoustic (PA) imaging emerged as a complementary technique, which uses light to induce detectable US waves *via* optical absorption and subsequent photothermal expansion. It combines the resolution and depth penetration of US with high contrast from selective optical absorption. When used with functional nanoconstructs, these modalities are a dynamic tool for early disease detection, molecular profiling, and therapy.[1] We have developed a triggerable nanosized US and PA contrast agent containing only biocompatible materials: a perfluorocarbon (PFC) nanodroplet loaded with indocyanine green (ICG) dye. We demonstrated that these particles produce three distinct forms of contrast, resulting from vaporization (PA signal), from thermoelastic expansion (PA signal), and from acoustic backscatter (US signal). Overall, the nanodroplets provide a triggerable platform to enhance PA and US contrast that is safe and potentially clinically translatable.

Gaseous PFC microbubbles are a common US contrast agent, and several formulations are commercially available for diagnostic imaging.[2] The bubbles provide contrast through an acoustic impedance mismatch or resonance,[3−5] and they assist cavitation for therapy.[6−9] Alternatively, liquid PFC nanodroplets are smaller and, therefore, have potentially longer *in vivo* stability and the capability to extravasate from leaky tumor vasculature.[10−14] Stability depends largely on droplet size, shell

* Address correspondence to emelian@mail.utexas.edu.

Received for review July 10, 2013 and accepted December 4, 2013.

Published online December 04, 2013
10.1021/nn403527r

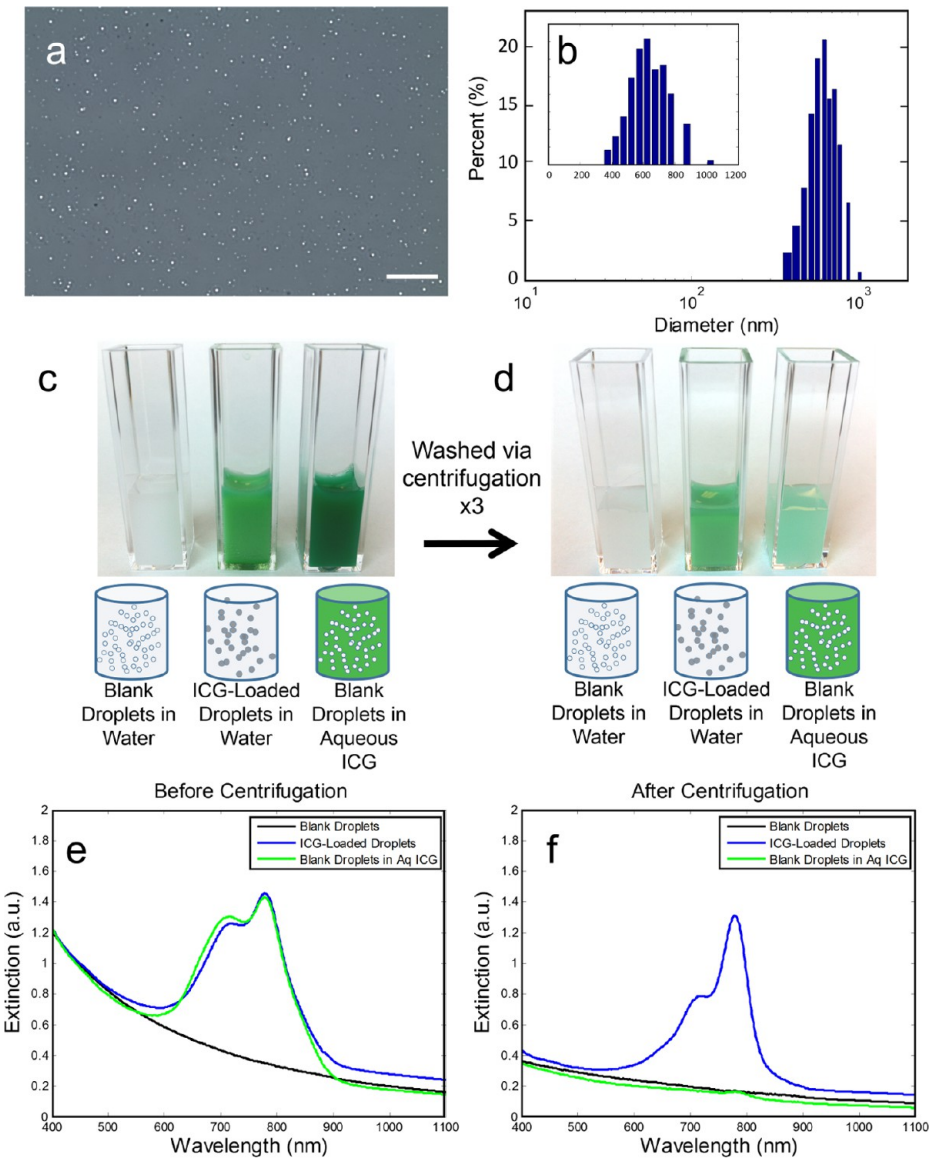

Figure 1. (a) Phase microscopy image of ICG-loaded PFC nanodroplets in water. (b) Size distribution of the droplets measured by dynamic light scattering. Photographs and diagrams of (c) prepared and (d) washed samples (from left to right): blank droplets in water, ICG-loaded droplets in water, and blank droplets in aqueous ICG. Extinction spectra of the samples (e) before and (f) after washing. Scale bar = 20 μm.

material, and most importantly, PFC boiling point.[15] Chemically inert PFC droplets have been safely used in oxygen transport as a blood substitute.[16] Drugs such as paclitaxel and doxorubicin may be incorporated in the droplet shell, rendering the droplets therapeutic delivery vehicles.[17−20] Lastly, droplets can be vaporized *via* high-intensity US,[21−24] providing triggered US contrast and drug release.

Recently, PFC droplets have encapsulated optical absorbers to achieve laser-triggered phase transition of PFC. Laser irradiation provides a safer, more controlled method of vaporization, using less energy than high-intensity US.[25,26] Upon pulsed laser irradiation, the region surrounding the optical absorber experiences both a temperature increase and a propagating pressure wave,[27] causing a liquid-to-gas phase transition of the droplet and inducing a one-time, high amplitude PA signal due to bubble formation. The resulting PFC bubble can provide US contrast either by acoustic impedance mismatch between the particles' gaseous core and the surrounding tissue and blood or by utilizing the bubble resonance frequency. To initiate vaporization of PFC, gold nanorods and lead sulfide nanoparticles were used previously, but these nanoconstructs are in experimental stages and their clinical translation will require extensive safety evaluation and regulatory approval.[25,26]

As an alternative, we propose to replace metallic nanoparticles with ICG to act as photoabsorber. Indeed, indocyanine green is approved to be injected for measuring cardiac output, hepatic function and for ophthalmic angiography.[28] It has been used in tens of

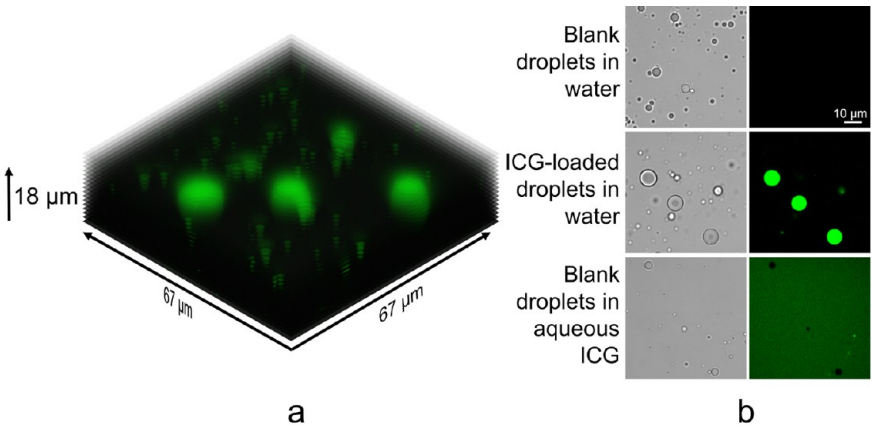

Figure 2. (a) Three-dimensional rendering of confocal fluorescence microscope images of ICG-loaded droplets in water. (b) Confocal microscope images of central cross sections of the three droplet samples, indicating the location of dye. Slice thickness = 1.0 μm.

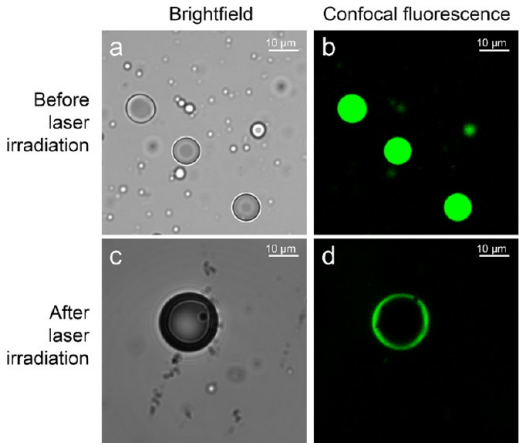

Figure 3. (a) Brightfield and (b) confocal fluorescence microscope images of ICG-loaded droplets through central cross sections before laser irradiation. (c) Brightfield and (d) confocal fluorescence images through central cross sections of particles after laser irradiation. Slice thickness = 1.0 μm.

thousands of patients with rare (<0.15%) side effects,[29,30] and the high absorption cross-section of ICG in the near-infrared range provides utility in the biological optical window, where attenuation due to endogenous chromophores is minimal.[31,32] Therefore, we investigated the possibility to encapsulate ICG dye within PFC droplets to create a safe, biocompatible, multifunctional contrast agent with the future goal of clinical translation. We first synthesized ICG-loaded PFC nanodroplets, and then we measured their optical absorption spectrum—before and after washing by centrifugation—to determine the retention of ICG by our nanoconstructs, which was confirmed by confocal microscopy. We demonstrated optically triggered enhanced PA contrast through vaporization and US contrast from the resulting bubbles. Furthermore, because of PFC's low boiling point (29 °C) relative to body temperature, we studied the effect of surrounding temperature on droplet vaporization and enhancement of PA and US signals.

RESULTS AND DISCUSSION

Nanodroplet Characterization. The synthesized ICG-loaded droplets were characterized to assess their utility in US and PA imaging and compared to blank droplets in aqueous ICG. The phase microscopy image of the droplets gives a qualitative view of the larger droplets in the sample (Figure 1a), and the distribution of their diameters was measured by dynamic light scattering (Figure 1b). The encapsulation efficiency of ICG in the droplets was 75%, with a payload of 0.58 mg of ICG per milliliter of sample. As made, the sample contains approximately 10^9 droplets/mL, yielding 5.8×10^{-10} mg ICG per droplet. The average droplet size was 600 nm with a dispersity of 0.28 (Methods). It is known that tumor neovasculature contains endothelial gap junctions up to 800 nm,[33] which may allow even these relatively large particles to passively accumulate in the tumor region *via* the enhanced permeability and retention effect.[34,35]

Indeed, droplet size is influenced by BSA concentration, sonication time and power, as well as filter pore size during extrusion. For example, nanodroplets have been created with average diameters ranging from 200 to 1000 nm.[36] In our studies, focused on demonstration of US and PA signal enhancement from ICG-loaded nanodroplets, the imaging results are reported from nanodroplets with a 600 nm average diameter.

To ensure that ICG was in the droplet PFC core, rather than dissolved in the aqueous solvent or adherent to the BSA shell, three samples of droplets were synthesized, similar to those previously mentioned, but larger in diameter, and imaged using confocal microscopy to identify the location of dye within the solution. Images in Figure 2 indicate that the ICG is distributed throughout the PFC core of the particles when loaded using the reported method, whereas blank droplets in aqueous ICG do not encapsulate the dye within the particle.

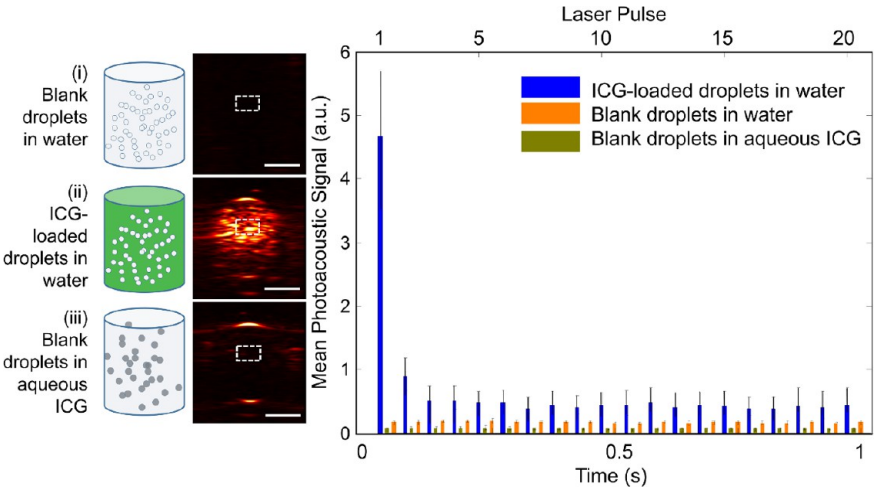

Figure 4. Diagram and PA image from the first laser pulse irradiating the samples of (i) blank droplets in water, (ii) ICG-loaded droplets in water, and (iii) blank droplets in aqueous ICG. Average PA intensity, measured in the denoted ROI, over a number of laser pulses (20 pulses/s) or time. Error bar represents 1 standard deviation above and 1 standard deviation below the mean value. $N \geq 3$ for all reported values, 37 °C, scale bar = 2 mm.

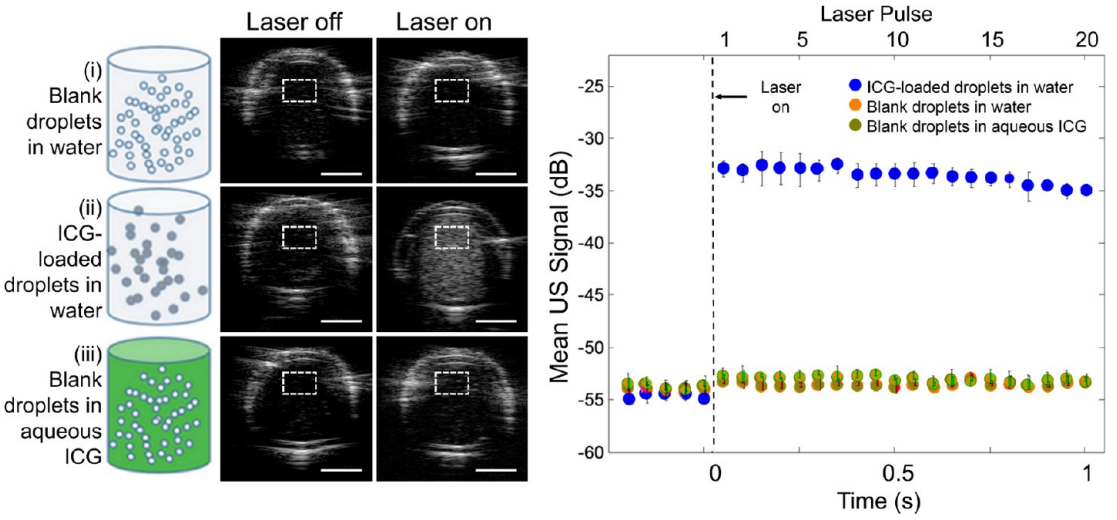

Figure 5. Ultrasound images before and after laser irradiation of samples of (i) blank droplets in water, (ii) ICG-loaded droplets in water, and (iii) blank droplets in aqueous ICG (50 dB display dynamic range), and average US intensity in the ROI for each US frame. Error bar represents 1 standard deviation above and 1 standard deviation below the mean value. $N \geq 3$ for all reported values, 37 °C, scale bar = 2 mm.

Additionally, the mass of ICG in the droplets before and after washing was measured using optical spectrometry. The ICG dye was added to a blank droplet solution until it reached equivalent optical density (OD) (1 cm path length) to that of the ICG-loaded droplets (Figure 1e). After washing *via* centrifugation three times, the ICG-loaded droplets did not lose color, but the blank droplets in aqueous ICG did (Figure 1d). The peak OD of the loaded droplets was 75% of its original value after washing, and the OD of blank droplets in aqueous ICG fell below the OD of blank droplets in water caused by scattering alone (Figure 1f). These measurements indicate that some ICG is adherent to the droplet's BSA shell, which is expected due to the affinity of ICG to albumin.[37] However, the encapsulation method ensures that nearly all of the ICG added to the emulsion *via* solvent evaporation is present after washing, which is paramount to optically triggered vaporization.

Upon pulsed laser irradiation, the dye-loaded droplets convert to bubbles through a liquid-to-gas phase transition induced optically. Under confocal microscopy, the dye shows a distinct rim pattern on a plane through the center of the particle, suggesting the attachment of the ICG to the albumin shell upon vaporization (Figure 3d).

Photoacoustic and Ultrasound Imaging of Nanodroplets. The photoacoustic contrast enhancement through droplet vaporization is shown after the initial laser pulse, and the average signal is quantified over several pulses (Figure 4). A Vevo LAZR imaging system was used to simultaneously collect US and PA data from the

TABLE 1. Quantified Image Enhancement[a]

	before lasing			during lasing		
	23 °C	37 °C	50 °C	23 °C	37 °C	50 °C
	Average Ultrasound Measurements ± 1× Standard Deviation					
Contrast (a.u)	1.0 ± 0.03	1.2 ± 0.06	1.7 ± 0.09	6.1 ± 0.2	14 ± 0.3	19 ± 0.3
CNR (dB)	20 ± 1.1	21 ± 0.8	23 ± 2.1	38 ± 0.1	46 ± 0.4	47 ± 1.1
	Average Photoacoustic Measurements ∓ Standard Deviation					
Contrast (a.u)	N/A	N/A	N/A	12 ± 5.6	36 ± 11	49 ± 18
CNR (dB)	N/A	N/A	N/A	41 ± 4.7	51 ± 6.2	55 ± 8.6

[a] Contrast and contrast-to-noise ratio for ultrasound and photoacoustic signal before and during pulsed laser irradiation of ICG-loaded droplets. Values reported are mean values ±1× standard deviation. $N \geq 3$ for all reported values. N/A = not applicable.

samples, using a laser emitting 780 nm light at a fluence of 20 mJ cm^{-2}. Photoacoustic images of a sample containing either (i) washed blank droplets in water, (ii) washed ICG-loaded droplets in water, or (iii) unwashed blank droplets in aqueous ICG (Figure 1c) were measured. Upon irradiation, the blank droplets in water emitted no PA signal that was detectable (*i.e.*, the signal was below the system noise). However, for ICG-loaded droplets, the PA signal due to vaporization was 10x higher than that of the system noise, indicating that the dye encapsulated inside the droplet is an effective optical trigger, and the particles are a source of high PA signal. There was no detectable PA signal from blank droplets in aqueous ICG, indicating that an equivalent amount of ICG outside the droplets does not induce vaporization. The PA and US images were further acquired for subsequent laser pulses—a movie made up of US and PA images of the sample of ICG-loaded droplets and blank droplets in aqueous ICG during irradiation is included in the Supporting Information (Movie S1). In each image, PA signal was averaged over a 0.23 mm^2 region of interest (ROI) to demonstrate droplet behavior as a function of laser pulse over 1 s (Figure 4). Upon irradiation, the PA image contrast is 36 (au), and the contrast-to-noise ratio (CNR) is 51 dB, compared to 1.1 (au) and 19 dB, respectively, for blank droplets in aqueous ICG. Subsequent laser pulses result in substantially lower PA signal, because very few additional droplets vaporize from these pulses. Almost all droplets that are large enough to vaporize within the sample undergo this phase transition after a single pulse.

To verify droplet vaporization and assess contrast enhancement, B-mode US data were collected from the same three samples, both before and during laser irradiation. As expected, US images of the ICG-loaded droplets exhibit a drastic increase in US contrast upon irradiation, which is absent in the other two samples of blank droplets (Figure 5). The US contrast increases from 1.2 to 14 (au), and the CNR increases from 21 to 46 dB (Table 1). In its liquid droplet form, the PFC adds little US contrast to an aqueous background because of its similar acoustic impedance. However, upon optical triggering of an ICG-loaded PFC-droplet, the acoustic impedance of gaseous PFC increases due to a substantial decrease in density and speed of sound, as indicated by the change in US contrast.

The fate of the encapsulated dye after droplet vaporization has implications for drug delivery and long-term imaging. Confocal fluorescence microscopy before and after laser irradiation confirms that the ICG, after activation, adheres to the albumin bubble shell (Figure 3). In related work, Reznik *et al.* found that a fluorescent dye, which was originally confined to the PFC core, attached to the shell of the bubble upon acoustic vaporization.[24] Given the short lifetime of PFC bubbles *in vivo*,[17] the dye will likely be bound to albumin after dissolution of PFC gas from the bubble core, and the albumin would be rapidly taken up by liver cells.[38]

The PA signal approaches baseline level quickly after the first laser pulse (Figure 4), whereas the US signal enhancement persists (Figure 5). The bulk of the irradiated droplets are vaporized after the first laser pulse, inducing a drastic but transient peak in PA signal.[25,26] Signal upon subsequent pulses can be attributed to one or a combination of the following: first, droplets in the solution may drift into the path of the laser beam and vaporize, causing additional PA signal. Alternatively, some of the smaller more stable droplets may require two or more laser pulses before vaporizing. So even if the majority vaporize after one pulse, a small signal can be seen in subsequent pulses. Ultrasound contrast, however, continues as long as the vaporized PFC bubbles are present. In this experimental setup, the bubbles provide contrast until they eventually float to the top of the sample over several seconds. In biological applications, the structure of the surrounding tissue would inhibit the bubbles from drifting, and the enhanced US contrast would last until the gas is dissolved and exhaled or the bubbles circulate out of the ROI.[39]

Several factors may contribute to the likelihood of a droplet vaporizing, including droplet size,[17] PFC

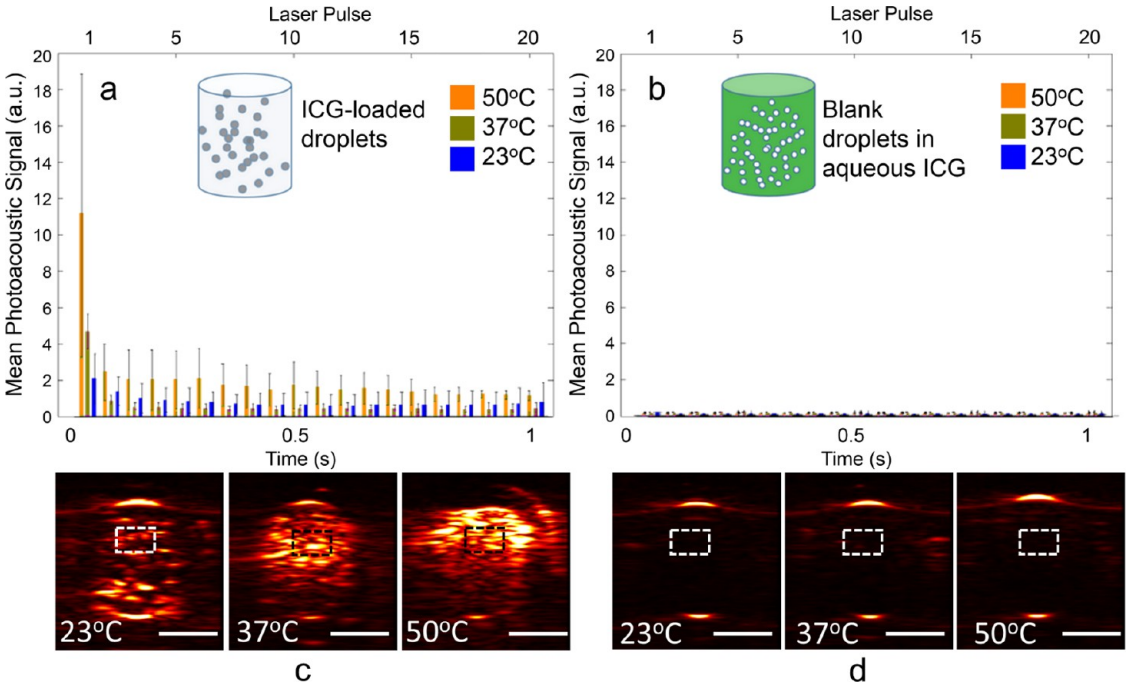

Figure 6. (a and b) Average PA intensity in the ROI from ICG-loaded droplets, and for blank droplets in aqueous ICG over 20 laser pulses and equivalent time. (c and d) Photoacoustic images of the pipet cross section after the first laser pulse, observed at three temperatures, for ICG-loaded droplets and blank droplets in aqueous ICG. Error bar represents 1 standard deviation above and 1 standard deviation below the mean value. $N \geq 3$ for all reported values. Scale bar = 2 mm.

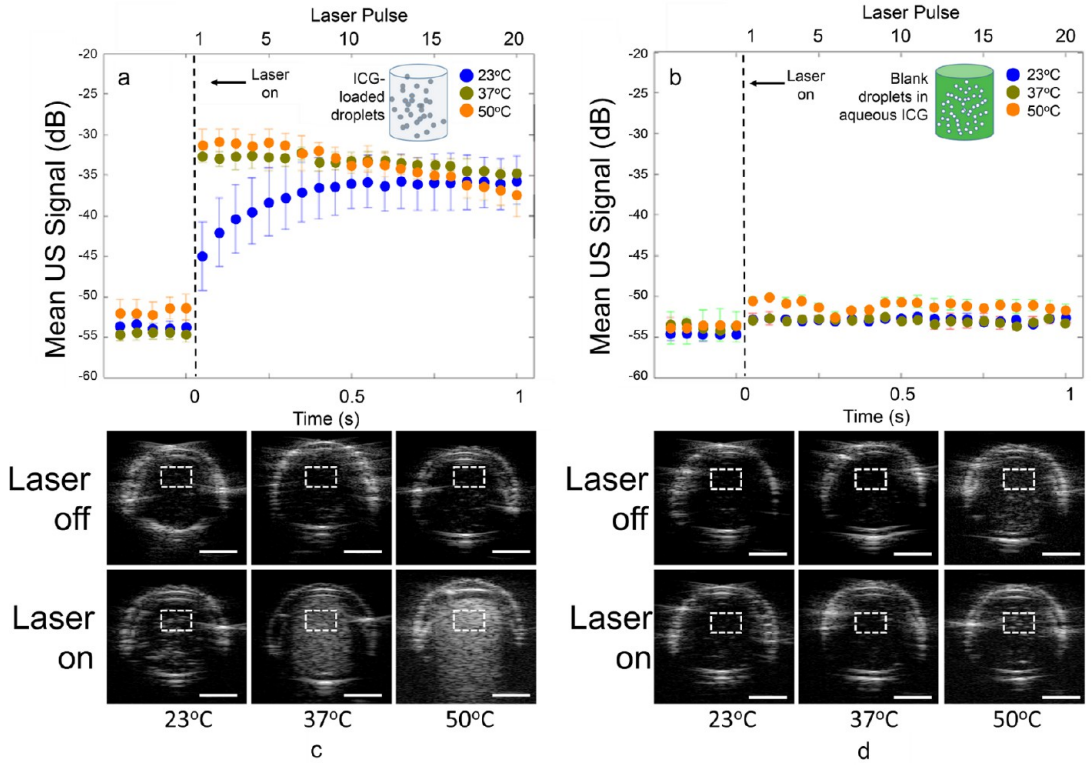

Figure 7. (a and b) Average US signal in the ROI before and after laser irradiation over each pulse and equivalent time for ICG-loaded droplets and blank droplets in aqueous ICG, displayed on a 50 dB scale. (c and d) Ultrasound images at three temperatures before and during laser irradiation for ICG-loaded droplets and blank droplets in aqueous ICG. Error bar represents 1 standard deviation above and 1 standard deviation below the mean value. $N \geq 3$ for all reported values. Scale bar = 2 mm.

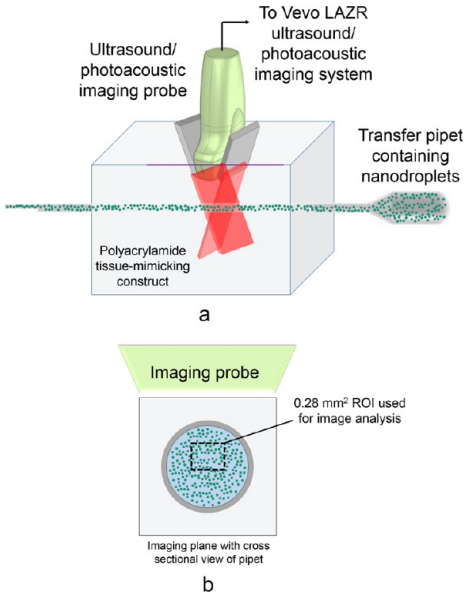

Figure 8. Imaging setup for nanodroplet samples, using a Vevo LAZR dual US/PA imaging system.

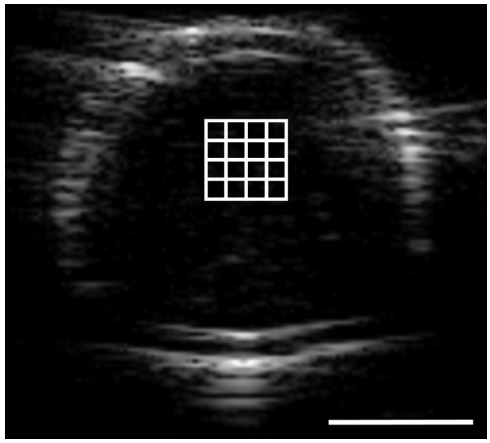

Figure 9. Ultrasound image depicted with the subsectioned ROI used for signal analysis.

boiling point,[15] photoabsorber encapsulation, external US field,[21] local laser fluence,[25] viscoelasticity of the medium, droplet shell composition,[40] and ambient temperature.[15] It is hypothesized that increasing the photoabsorber concentration, in this case ICG, would increase both US and PA contrast initially due to increased likelihood of vaporization, up to a point when all droplets are vaporized. It is also possible that increased rate or volume of expansion during vaporization leads to increased US and PA contrast. The imaging experiments reported in Figures 4 and 5 were performed at 37 °C; we further investigated the effect of ambient temperature on the PA signal produced by droplet vaporization, and on the US contrast from the resulting bubbles. The boiling point of this particular PFC is 29 °C, rendering it liquid at room temperature but gaseous at body temperature. However, when the albumin surfactant is used to make nanodroplets, the PFC does not vaporize at body temperature, due to Laplace pressure imposed at the particle boundary.[17] This renders the PFC a superheated liquid at 37 °C, and the particles remain nanodroplets rather than bubbles.

Effect of Temperature on PA and US Image Contrast. Samples of ICG-loaded droplets and of blank droplets in aqueous ICG were imaged using PA and US techniques at three different temperatures: room temperature (23 °C) to observe the effect of irradiation on droplets well below their boiling point; body temperature (37 °C) to study biologically relevant conditions; and 50 °C to observe the effects of further superheating the droplets. Photoacoustic images and signal averages at all temperatures are shown in Figure 6. The PA signal from ICG-loaded droplets over time is accompanied by images from the first laser pulse for each temperature (Figure 6a,c). At increased temperatures, the nanodroplets produce greater PA signal upon vaporization. For the blank droplets in aqueous ICG, there was no detectable PA signal at any temperature. Each sample contained droplets ranging in diameter from approximately 200 nm up to 1 μm, and the Laplace pressure on a small droplet may significantly increase its boiling point.[17] At lower temperatures, the laser fluence is insufficient to vaporize all (*i.e.*, the smaller) droplets. At higher temperatures, the PFC is superheated and volatile, so a laser pulse of the same fluence vaporizes a greater percentage of the irradiated droplets, producing a higher average PA signal. Alternatively, volume or rate of particle expansion during irradiation is greater at increased temperatures, inducing stronger PA signal. This increased signal at high temperatures can be exploited to maximize contrast using this imaging technique. To do so, factors such as the type of PFC (and thus boiling point), droplet size and shell stiffness, and laser fluence may be adjusted. It is noted that at 50 °C, the PA signal is small but detectable (*i.e.*, above the noise level of the system) during the subsequent laser pulses, while at other temperatures the PA signal is detected from only the first pulse. At 50 °C, surrounding droplets in aqueous solution are likely to enter the imaging plane due to flow caused by vaporization. These introduced droplets undergo vaporization, prolonging the elevated PA signal in the subsequent pulses. This is also evident in a movie showing vaporization (Supporting Information, Movie S1). However, it is unlikely to be a significant phenomenon in clinical imaging conditions if the nanodroplets are imaged outside of the vascular compartments.

The US signal from ICG-loaded droplets is shown over time with images before and after irradiation (Figure 7a, 7c). The gradual decrease in US signal over time at higher temperatures can likely be attributed to the bubbles slowly floating out of the ROI, and possibly

to acoustic shadowing, as seen in the Supporting Information Movie S1. The gradual increase in US signal for droplets at room temperature is likely because fewer droplets vaporize, but the bubbles float and accumulate within the ROI. The US and PA contrast and CNR at all temperatures can be seen in Table 1. Dye-loaded droplets at all temperatures exhibit significant increases in contrast and CNR ($p < 0.001$). The enhanced contrast at higher temperatures is likely due either to greater vaporization efficiency, rate of particle expansion, or volume of expansion. For blank droplets in aqueous ICG, there is no significant US contrast increase for the samples at 23 and 37 °C, and the US signal increases modestly but significantly (2.9 dB) upon irradiation at 50 °C ($p < 0.05$).

The developed nanodroplets may be targeted for functional, cellular and molecular imaging.[41] The release of dye may be used for optical imaging of cancers in dense breast tissue or of metastasis in the sentinel lymph nodes.[42,43] The extinction spectrum of ICG is dynamic; its absorption peak shifts in response to changes in concentration and background environment, suggesting its use as an indicator of nanodroplet vaporization and subsequent release of encapsulated therapeutics.[44] In addition, chemotherapeutic drug release upon vaporization may localize treatment of tumors,[17−19] and delivery may be improved by sonoporation with high intensity US.[7,9] The cytotoxicity of similar particles has been studied, and it was determined that PFC nanodroplets with encapsulated gold nanorods exhibit no significant toxicity to pancreatic cancer cells.[26] From this data, and the biocompatibility of indocyanine green dye,[29,30,43] it is highly unlikely that the nanoconstruct proposed in this work would present any adverse biological effects.

CONCLUSIONS

In conclusion, we have developed a nanoconstruct entirely from biocompatible materials, which enhances contrast in PA and US images in response to an external optical trigger. We characterized the PA and US signal generation from the developed nanoconstructs and several control nanodroplets, and we studied their behavior at varying temperatures. Our studies suggest that these nanodroplets may become a valuable tool for various imaging modalities, and have promising therapeutic applications.

METHODS

Preparation of ICG-Loaded Perfluorocarbon Nanodroplets. An emulsion of blank droplets consisting of a perfluorocarbon core surrounded by an albumin shell was first synthesized. First, 2.7 mL of 2 mg/mL bovine serum albumin (BSA) (Sigma) kept at 10 °C was added to an 8 mL glass scintillation vial. Next, 0.3 mL of perfluoropentane (Dodecafluoropentane) C_5F_{12} (FluoroMed) (PFP) was added to the vial. This solution was kept on ice to prevent evaporation of the PFP during creation of the emulsion, which has a boiling point of 29 °C. Next, the vial was shaken using Mini Vortexer (VWR) on speed setting 10 for 10 s, to emulsify the PFP into submillimeter diameter droplets. An ultrasonic cleaner (VWR) was filled with water at 10 °C, and the vial was sonicated in the tank at 180 W for 3 min, while the vial was simultaneously shaken by hand, to emulsify the solution as much as possible and to disrupt the droplets into smaller sizes. A slight excess of PFP in the solution formed a bolus in the bottom of the vial, so ~2.5 mL of the 3 mL droplet solution was transferred to another 8 mL glass vial, excluding the bolus of PFP. After emulsification into a nanodroplet size, the Laplace pressure increases the boiling point of the droplets to 70 °C or higher, depending on size.[45,46]

The ICG was encapsulated in the droplets using a modified method by Rodriguez *et al.*[47] A 1 mL solution of 2 mM ICG in chloroform was made by adding powdered ICG (Cardiogreen) (Sigma) to chloroform (Sigma). Depending on ICG supplier, the addition of approximately 0.2 mL of Tween 20 (Calbiochem) may be necessary to assist the dissolution of ICG. A separate 1 mL solution of 12 mM tetrabutylammonium iodide (TBAI) (Acros) in chloroform was made similarly. The 1 mL solution of TBAI was added to the ICG solution, resulting in a 1 mM ICG and 6 mM TBAI solution in chloroform. The solution was sonicated using a VWR Ultrasonic Cleaner at 180 W for 30 min.

The glass vial of blank droplets was placed on a stir plate and stirred at 1200 rpm, while 2 mL of the ICG-TBAI solution in chloroform was added dropwise. Next, a vacuum tube was attached to the top of the vial, and the chloroform was evaporated from the solution. Chloroform, whose bulk boiling point is 61 °C, evaporates more readily under vacuum than do the PFC droplets, most of which have a boiling point above 70 °C.[45,46] All observable chloroform was evaporated from the emulsion, requiring approximately 30 min. A green-colored, milky solution of droplets remained. This solution was transferred to a 2.5 mL plastic centrifugation tube and centrifuged at 200*g* for 5 min using a MiniSpin plus centrifuge (Eppendorf). After centrifugation, a dark green pellet of droplets formed at the bottom of the tube, and the light green supernatant was discarded. The supernatant was replaced with water at 10 °C, and the droplets were resuspended by shaking in the Vortexer and sonicating in the VWR benchtop sonicator set at 180 W for 3 min. The solution was washed three times in this fashion, and the supernatant was colorless at the end of the third centrifugation. The droplet emulsion as made was diluted by 1000× in saline before experimentation, yielding a final droplet concentration of 10^6 droplets/mL and a dye payload of 0.58 μg/mL of ICG.

Microscopy. The droplets were imaged using a Leica DMI 3000B inverted light microscope (Leica Microsystems) in phase using a 40× objective. The droplet emulsion as made were diluted 20× in water, and 10 μL of the dilution was placed onto a microscope slide, with a glass coverslip placed over it. Confocal microscopy was performed using an LSM 710 confocal microscope (Zeiss).

Spectrophotometry. To measure the extinction spectrum of the droplets, a UV-3600 UV−vis Spectrophotometer (Shimadzu) was used. The droplet emulsion as made was diluted approximately 50× in water and placed into a plastic cuvette with a 1 cm path length for spectral analysis.

Size Measurement by Dynamic Light Scattering. For measurement of droplet size, the ICG-loaded droplets were analyzed using a Delsa Nano Submicrometer particle analyzer (Beckman Coulter). The instrument collected data and analyzed particle size, directly outputting real-time size data for the droplets. The fluctuations of light scattered by particles are analyzed using the autocorrelation function, which exhibits a curved line for polydisperse samples. In the Cumulants method, one fits the logarithm of the autocorrelation function to a polynomial to determine the coefficients. The first order coefficient is the

average decay constant, from which the average diffusion coefficient and particle diameter can be calculated by the definition of the diffusion coefficient and the Stokes–Einstein equation. The second order coefficient divided by the square of the decay constant is the polydispersity index, which is typically smaller than 0.1 for monodisperse samples and becomes larger for polydisperse samples.

Preparation of a Polyacrylamide Tissue-Mimicking Construct. To stabilize the transfer pipet during irradiation and for ease of imaging, we inserted it into a block made of polyacrylamide gel. To construct the gel, 64 mL of water was stirred at room temperature, and added to the water was 21 mL of 40% acrylamide (Ambion), 850 μL of ammonium persulfate (Sigma-Aldrich), and 106 μL of tetramethylethylenediamine (TEMED) (Sigma). The solution was poured into a mold which contained an inclusion to create a hole for the pipet. The phantom set in 20 min and was stored submerged in water in the refrigerator until ready for use.

Optical Irradiation and Collection of Ultrasound and Photoacoustic Data. The gel block was placed under the Vevo 21 MHz ultrasound and photoacoustic imaging probe, as depicted in Figure 8. The probe was connected to the combined ultrasound and photoacoustic VevoLAZR imaging system. Ultrasound gel was applied to the block and the probe was positioned so that the optical beams intersected at the position of the pipet and at the focal spot of the US transducer. Ultrasound B-mode data was collected from the cross section of the pipet without optical irradiation, in which droplet samples were suspended. The transmit power of the US wave was set to 1% to avoid or minimize any mechanical (*i.e.*, pressure) contribution to droplet vaporization (1% power ~350 kPa). The imaging system was operating in a single-focus imaging mode, with the ultrasound beam focused around 20 mm below the surface of the transducer. The pipet was placed so that its cross section spanned 9–13 mm range below the transducer. Because droplets are denser (1.6 g/mL) than the aqueous solvent, a new sample of droplets was aspirated into a pipet to prevent droplet settling within the pipet before PA imaging commenced. The pipet was inserted into the gel block, and the laser was turned on while US and PA data were simultaneously collected. The 780 nm wavelength, 5 ns laser pulses irradiated the sample at 20 pulses/s and a fluence of 20 mJ cm^{-2}, while US and PA frames were captured at a rate of one frame per laser pulse (20 frames/s). IQ B-mode data was collected for analysis of contrast enhancement by custom-designed programs developed in MATLAB.

Ultrasound and Photoacoustic Signal Analysis. To measure the mean US signal for a given laser pulse (frame), the signal was converted to dB, then averaged in the ROI. Each point in the graph is calculated by

$$\text{Mean US Signal} = \frac{\sum_{i=1}^{N} 20 \times \log_{10}(I_i)}{N}$$

where I_i is the normalized (by maximum pixel of all US images) linear intensity of each pixel in the ROI, and N is the total number of pixels in the ROI. This results in the plots shown in Figure 3b.

The selection of the ROI within the image frame (Figure 9) has an effect on the resulting measurement of mean US signal. Because acoustic shadowing occurs more at higher temperatures, there is a gradient of US signal intensity with depth (deeper → more shadowing → artificially lower signal). By selecting the ROI close to the top of the pipet, we minimize this effect and more accurately show that at 50 °C there is more vaporization than at 37 °C.

Using the same signals at various temperatures, we calculated the contrast and contrast-to-noise (CNR) for the ICG-loaded droplets:

$$\text{Contrast} = \left[\frac{\mu(I_{i,\,\text{bubbles}}) - \mu(I_{i,\,\text{background}})}{\mu(I_{i,\,\text{background}})}\right]$$

$$\text{CNR} = 20 \times \log_{10}\left[\frac{\mu(I_{i,\,\text{bubbles}}) - \mu(I_{i,\,\text{background}})}{\sigma(I_{i,\,\text{background}})}\right]$$

where I_i is the average linear US intensity in one of the 16 sub-ROIs in the US image, $\mu(I_{i,\ \text{bubbles}})$ is an average of 16 values of I_i, where each I_i is an average of all pixel values (linear US signal) in the small square. $I_{i,\ \text{background}}$ is calculated the same way, using an ROI (and 16 sub-ROIs) outside of the pipet region, and σ is the standard deviation of 16 values of I_i.

The values for contrast and CNR can be found in Table 1.

Because of the acoustic shadowing at 50 °C, there is greater signal variance within the frame than at 37 °C. This increase in "noise" artificially decreases the values of CNR for the 50 °C case.

Photoacoustic measurements were made in an identical fashion, but using the PA images from the first laser pulse as a measurement of signal rather than the US images. Several values of contrast and CNR were obtained by moving the ROI within the image. Averages and standard deviations of contrast and CNR can be found in Table 1.

Conflict of Interest: The authors declare the following competing financial interest(s): Stanislav Emelianov - Stockholder, Nanohybrids, Inc. Kimberly Homan - Chief Technology Officer, Nanohybrids, Inc.

Acknowledgment. Partial support from the Breast Cancer Research Foundation and National Institutes of Health under Grant CA171668 is acknowledged.

Supporting Information Available: A movie of PA and US signal due to vaporization of ICG-loaded droplets at body temperature (avi format). This material is available free of charge *via* the Internet at http://pubs.acs.org.

REFERENCES AND NOTES

1. Ferrari, M. Cancer Nanotechnology: Opportunities and Challenges. *Nat. Rev. Cancer* **2005**, *5*, 161–171.
2. Lindner, J. R. Microbubbles in Medical Imaging: Current Applications and Future Directions. *Nat. Rev. Drug Discovery* **2004**, *3*, 527–533.
3. Goldberg, B. B.; Liu, J.-B.; Forsberg, F. Ultrasound Contrast Agents: A Review. *Ultrasound Med. Biol.* **1994**, *20*, 319–333.
4. Frinking, P. J.; Bouakaz, A.; Kirkhorn, J.; Ten Cate, F. J.; Jong, N. De. Ultrasound Contrast Imaging: Current and New Potential Methods. *Ultrasound Med. Biol.* **2000**, *26*, 965–975.
5. Anderson, C. R.; Hu, X.; Tlaxca, J.; Decleves, A.-E.; Houghtaling, R.; Sharma, K.; Lawrence, M.; Ferrara, K.; Rychak, J. J. Ultrasound Molecular Imaging of Tumor Angiogenesis with an Integrin Targeted Microbubble Contrast Agent. *Invest. Radiol.* **2011**, *46*, 215.
6. Tran, B. C.; Seo, J.; Hall, T. L.; Fowlkes, J. B.; Cain, C. A. Microbubble-Enhanced Cavitation for Noninvasive Ultrasound Surgery. *IEEE Trans Ultrason. Ferroelectr. Freq. Control* **2003**, *50*, 1296–1304.
7. Lin, C.-Y.; Huang, Y.-L.; Li, J.-R.; Chang, F.-H.; Lin, W.-L. Effects of Focused Ultrasound and Microbubbles on the Vascular Permeability of Nanoparticles Delivered into Mouse Tumors. *Ultrasound Med. Biol.* **2010**, *36*, 1460–1469.
8. Wamel, A. Van; Kooiman, K.; Harteveld, M.; Emmer, M.; Ten Cate, F. J.; Versluis, M.; Jong, N. De. Vibrating Microbubbles Poking Individual Cells: Drug Transfer into Cells *via* Sonoporation. *J. Controlled Release* **2006**, *112*, 149–155.
9. Hannah, A.; Wilson, K.; Homan, K.; Emelianov, S. Ultrasound-Induced Cellular Uptake of Plasmonic Gold Nanorods. *Proc. SPIE* **2011**, *7899*, No. 789920.
10. Yuan, F.; Dellian, M.; Fukumura, D.; Leunig, M.; Berk, D. A.; Torchilin, V. P.; Jain, R. K. Vascular Permeability in a Human Tumor Xenograft: Molecular Size Dependence and Cutoff Size. *Cancer Res.* **1995**, *55*, 3752–3756.
11. Dayton, P. A.; Matsunaga, T. O. Ultrasound-Mediated Therapies Using Oil and Perfluorocarbon-Filled Nanodroplets. *Drug Dev. Res.* **2006**, *67*, 42–46.
12. Martin, A. L.; Seo, M.; Williams, R.; Belayneh, G.; Foster, F. S.; Matsuura, N. Intracellular Growth of Nanoscale Perfluorocarbon Droplets for Enhanced Ultrasound-Induced Phase-Change Conversion. *Ultrasound Med. Biol.* **2012**, *38*, 1799–1810.

13. Rapoport, N.; Christensen, D. A.; Kennedy, A. M.; Nam, K.-H. Cavitation Properties of Block Copolymer Stabilized Phase-Shift Nanoemulsions Used as Drug Carriers. *Ultrasound Med. Biol.* **2010**, *36*, 419–429.
14. Rapoport, N.; Nam, K.-H.; Gupta, R.; Gao, Z.; Mohan, P.; Payne, A.; Todd, N.; Liu, X.; Kim, T.; Shea, J. Ultrasound-Mediated Tumor Imaging and Nanotherapy Using Drug Loaded, Block Copolymer Stabilized Perfluorocarbon Nanoemulsions. *J. Controlled Release* **2011**, *153*, 4–15.
15. Sheeran, P. S.; Luois, S. H.; Mullin, L. B.; Matsunaga, T. O.; Dayton, P. A. Design of Ultrasonically-Activatable Nanoparticles Using Low Boiling Point Perfluorocarbons. *Biomaterials* **2012**, *33*, 3262–3269.
16. Riess, J. G.; Krafft, M. P. Fluorinated Materials for *in Vivo* Oxygen Transport (Blood Substitutes), Diagnosis and Drug Delivery. *Biomaterials* **1998**, *19*, 1529–1539.
17. Rapoport, N. Y.; Kennedy, A. M.; Shea, J. E.; Scaife, C. L.; Nam, K.-H. Controlled and Targeted Tumor Chemotherapy by Ultrasound-Activated Nanoemulsions/microbubbles. *J. Controlled Release* **2009**, *138*, 268–276.
18. Rapoport, N.; Gao, Z.; Kennedy, A. Multifunctional Nanoparticles for Combining Ultrasonic Tumor Imaging and Targeted Chemotherapy. *J. Natl. Cancer Inst.* **2007**, *99*, 1095–1106.
19. Nam, K.-H.; Christensen, D. A.; Kennedy, A. M.; Rapoport, N. Acoustic Droplet Vaporization, Cavitation, and Therapeutic Properties of Copolymer-Stabilized Perfluorocarbon Nanoemulsions. *AIP Conf. Proc.* **2009**, *1113*, 124.
20. Wang, C.-H.; Kang, S.-T.; Lee, Y.-H.; Luo, Y.-L.; Huang, Y.-F.; Yeh, C.-K. Aptamer-Conjugated and Drug-Loaded Acoustic Droplets for Ultrasound Theranosis. *Biomaterials* **2012**, *33*, 1939–1947.
21. Kripfgans, O. D.; Fowlkes, J. B.; Miller, D. L.; Eldevik, O. P.; Carson, P. L. Acoustic Droplet Vaporization for Therapeutic and Diagnostic Applications. *Ultrasound Med. Biol.* **2000**, *26*, 1177–1189.
22. Giesecke, T.; Hynynen, K. Ultrasound-Mediated Cavitation Thresholds of Liquid Perfluorocarbon Droplets *in Vitro*. *Ultrasound Med. Biol.* **2003**, *29*, 1359–1365.
23. Sheeran, P. S.; Dayton, P. A. Phase-Change Contrast Agents for Imaging and Therapy. *Curr. Pharm. Des.* **2012**, *18*, 2152–2165.
24. Reznik, N.; Seo, M.; Williams, R.; Bolewska-Pedyczak, E.; Lee, M.; Matsuura, N.; Gariepy, J.; Foster, F. S.; Burns, P. N. Optical Studies of Vaporization and Stability of Fluorescently Labelled Perfluorocarbon Droplets. *Phys. Med. Biol.* **2012**, *57*, 7205.
25. Strohm, E.; Rui, M.; Gorelikov, I.; Matsuura, N.; Kolios, M. Vaporization of Perfluorocarbon Droplets Using Optical Irradiation. *Biomed. Opt. Express* **2011**, *2*, 1432.
26. Wilson, K.; Homan, K.; Emelianov, S. Biomedical Photoacoustics beyond Thermal Expansion Using Triggered Nanodroplet Vaporization for Contrast-Enhanced Imaging. *Nat. Commun.* **2012**, *3*, 618.
27. Bell, A. G. On the Production and Reproduction of Sound by Light. *Am. J. Sci.* **1880**, 305–324.
28. Funovics, M.; Weissleder, R.; Tung, C.-H. Protease Sensors for Bioimaging. *Anal. Bioanal. Chem.* **2003**, *377*, 956–963.
29. Sakka, S. G. Assessing Liver Function. *Curr. Opin. Crit. Care* **2007**, *13*, 207–214.
30. Weissleder, R. A Clearer Vision for in *Vivo* Imaging. *Nat. Biotechnol.* **2001**, *19*, 316–316.
31. Jo, F. F. Discovery of the Near-Infrared Window into the Body and the Early Development of Near-Infrared Spectroscopy. *J. Biomed. Opt.* **1999**, *4*, 392–396.
32. Cherrick, G. R.; Stein, S. W.; Leevy, C. M.; Davidson, C. S. Indocyanine Green: Observations on Its Physical Properties, Plasma Decay, and Hepatic Extraction. *J. Clin. Invest.* **1960**, *39*, 592.
33. Hobbs, S. K.; Monsky, W. L.; Yuan, F.; Roberts, W. G.; Griffith, L.; Torchilin, V. P.; Jain, R. K. Regulation of Transport Pathways in Tumor Vessels: Role of Tumor Type and Microenvironment. *Proc. Natl. Acad. Sci. U.S.A.* **1998**, *95*, 4607–4612.
34. Torchilin, V. Tumor Delivery of Macromolecular Drugs Based on the EPR Effect. *Adv. Drug Delivery Rev.* **2011**, *63*, 131–135.
35. Iyer, A. K.; Khaled, G.; Fang, J.; Maeda, H. Exploiting the Enhanced Permeability and Retention Effect for Tumor Targeting. *Drug Discovery Today* **2006**, *11*, 812–818.
36. Wilson, K.; Homan, K.; Emelianov, S. Synthesis of a Dual Contrast Agent for Ultrasound and Photoacoustic Imaging. *Proc. SPIE* **2010**, *7576*, No. 75760M.
37. Landsman, M. L.; Kwant, G.; Mook, G. A.; Zijlstra, W. G. Light-Absorbing Properties, Stability, and Spectral Stabilization of Indocyanine Green. *J. Appl. Physiol.* **1976**, *40*, 575–583.
38. Fujita, T.; Nishikawa, M.; Ohtsubo, Y.; Ohno, J.; Takakura, Y.; Sezaki, H.; Hashida, M. Control of in *Vivo* Fate of Albumin Derivatives Utilizing Combined Chemical Modification. *J. Drug Targeting* **1994**, *2*, 157–165.
39. Lowe, K. C. Fluorinated Blood Substitutes and Oxygen Carriers. *J. Fluorine Chem.* **2001**, *109*, 59–65.
40. Reznik, N.; Williams, R.; Burns, P. N. Investigation of Vaporized Submicron Perfluorocarbon Droplets as an Ultrasound Contrast Agent. *Ultrasound Med. Biol.* **2011**, *37*, 1271–1279.
41. Kaneda, M. M.; Caruthers, S.; Lanza, G. M.; Wickline, S. A. Perfluorocarbon Nanoemulsions for Quantitative Molecular Imaging and Targeted Therapeutics. *Ann. Biomed. Eng.* **2009**, *37*, 1922–1933.
42. Murawa, D.; Hirche, C.; Dresel, S.; Hünerbein, M. Sentinel Lymph Node Biopsy in Breast Cancer Guided by Indocyanine Green Fluorescence. *Br. J. Surg.* **2009**, *96*, 1289–1294.
43. Intes, X.; Ripoll, J.; Chen, Y.; Nioka, S.; Yodh, A. G.; Chance, B. *In Vivo* Continuous-Wave Optical Breast Imaging Enhanced with Indocyanine Green. *Med. Phys.* **2003**, *30*, 1039.
44. Rajian, J. R.; Fabiilli, M. L.; Fowlkes, J. B.; Carson, P. L.; Wang, X. Drug Delivery Monitoring by Photoacoustic Tomography with an ICG Encapsulated Double Emulsion. *Opt. Express* **2011**, *19*, 14335.
45. Barber, E. J.; Cady, G. H. Vapor Pressures of Perfluoropentanes. *J. Phys. Chem.* **1956**, *60*, 504–505.
46. Rapoport, N. Y.; Efros, A. L.; Christensen, D. A.; Kennedy, A. M.; Nam, K.-H. Microbubble Generation in Phase-Shift Nanoemulsions Used as Anticancer Drug Carriers. *Bubble Sci., Eng., Technol.* **2009**, *1*, 31.
47. Rodriguez, V. B.; Henry, S. M.; Hoffman, A. S.; Stayton, P. S.; Li, X.; Pun, S. H. Encapsulation and Stabilization of Indocyanine Green within Poly(styrene-alt-maleic anhydride-)block-poly (styrene) Micelles for near-Infrared Imaging. *J. Biomed. Opt.* **2008**, *13*, No. 014025.